

Critical behavior of drops in linear flows. I. Phenomenological theory for drop dynamics near critical stationary states

Jerzy Bławdziewicz

Department of Mechanical Engineering, Yale University, New Haven, Connecticut 06520-8286

Vittorio Cristini^{a)} and Michael Loewenberg

Department of Chemical Engineering, Yale University, New Haven, Connecticut 06520-8286

(Received 5 March 2002; accepted 19 April 2002; published 1 July 2002)

The dynamics of viscous drops in linear creeping flows are investigated near the critical flow strength at which stationary drop shapes cease to exist. According to our theory the near-critical behavior of drops is dominated by a single slow mode evolving on a time scale that diverges at the critical point with exponent 1/2. The theory is based on the assumption that the system undergoes a saddle-node bifurcation. The predictions have been verified by numerical simulations for drops in axisymmetric straining flow and in two-dimensional flows with less vorticity than in shear flow. Application of our theory to the accurate determination of critical parameters is discussed. © 2002 American Institute of Physics. [DOI: 10.1063/1.1485076]

I. INTRODUCTION

Emulsion properties, such as rheology, depend strongly on the drop size distribution. Thus, it is important to understand and predict drop breakup in creeping flows, and there has been much research on this topic (as reviewed by Stone¹). Recent studies include drop breakup in stationary,^{2–6} and time-dependent^{7–12} flows. Some of the research has been focused on the criteria for breakup and some on the drop fragments produced by individual breakup events.

In stationary flows, criteria for breakup can be expressed in terms of a critical capillary number, i.e., the (dimensionless) flow strength above which no stationary drop shapes exist. The critical capillary number depends on the form of the flow and the viscosity ratio of the drop. In transient flows, criteria for breakup also depend on the flow history and the initial drop shape.

Recently, Navot¹³ explored drop dynamics in a stationary axisymmetric straining flow under conditions close to the critical capillary number. Using numerical simulations, Navot demonstrated that the time scale for drop evolution diverges at the critical capillary number with exponent 1/2, and the stationary drop length exhibits a nonanalytical, square-root behavior in the near-critical regime. The main features of the near-critical drop behavior were qualitatively explained using a simple one-parameter model with drop shape parametrized by drop length.

In a recent presentation,¹⁴ we reported similar observations and described a systematic analysis of drop dynamics under near-critical conditions. We showed that in the near-critical regime, a one-parameter description of drop-shape evolution holds because of the separation of time scales. The slow time scale corresponds to a single critical mode that

becomes unstable at the critical capillary number. The remaining stable modes evolve on a fast time scale; thus, at long times, they adiabatically follow the evolution of the critical slow mode. The details of this analysis are described herein.

II. DEFORMABLE DROPS IN LINEAR FLOWS

A. Velocity field

We consider the evolution of a viscous drop with volume $\frac{4}{3}\pi a^3$ immersed in an unbounded fluid undergoing stationary Stokes flow. The viscosity of the continuous phase is μ_1 and the drop phase is $\mu_2 = \eta^{-1}\mu_1$. The drop interface has constant interfacial tension σ .

A linear external velocity field is assumed

$$\mathbf{v}_0 = \dot{\gamma} \mathbf{D} \cdot \mathbf{r}, \quad (1)$$

where \mathbf{r} is the position, $\dot{\gamma}$ is the magnitude of the flow, and \mathbf{D} is the normalized velocity-gradient tensor.

The fluid velocity \mathbf{v} and pressure p in phase (i) satisfy the Stokes equations

$$\mu_i \nabla^2 \mathbf{v} - \nabla p = 0, \quad \nabla \cdot \mathbf{v} = 0. \quad (2)$$

At the drop interface S , velocity field and tangential stresses are continuous, and the jump of normal stresses across S is equal to the capillary pressure

$$[\mathbf{n} \cdot \boldsymbol{\tau} \cdot \mathbf{n}]_S = 2C\sigma \mathbf{n}, \quad (3)$$

where $\boldsymbol{\tau}$ is the stress tensor, \mathbf{n} is the outwards normal vector, and C is the local mean curvature. At infinity, the velocity field \mathbf{v} satisfies the boundary condition

$$\mathbf{v} = \mathbf{v}_0. \quad (4)$$

According to Eqs. (1)–(4), drop evolution depends on the viscosity ratio η , the capillary parameter

^{a)}Present address: Department of Chemical Engineering and Materials Science, University of Minnesota, 421 Washington Avenue S.E., Minneapolis, MN 55455-0132.

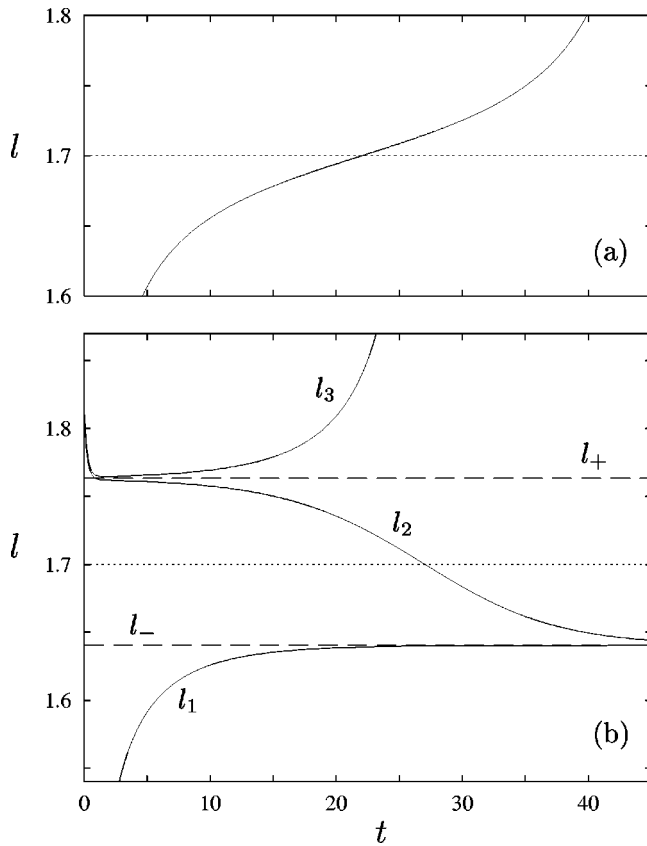


FIG. 1. Drop length versus time for initially spheroidal drops ($\eta=1$) in axisymmetric strain; $\kappa/\kappa_C=0.998$ (a) and $\kappa/\kappa_C=1.004$ (b), where κ_C is given by Eq. (48). Drop length evolution with different initial conditions (solid lines); stationary drop lengths l_{\pm} (dashed lines); critical length l_0 (dotted line).

$$\kappa = \frac{\sigma}{a\mu_1\dot{\gamma}} \tag{5}$$

(the inverse capillary number), and four dimensionless parameters characterizing form of external flow. In the present paper, we examine the dependence of drop evolution on κ , for given η and external flow type.

B. Evolution of the drop shape

To characterize the instantaneous drop shape, we introduce an array of shape parameters \mathbf{f} . (An example is the set of expansion coefficients of the radial coordinate of the interface into spherical harmonics.^{15,16}) The general arguments presented in this paper, however, are independent of the particular choice of \mathbf{f} .

The evolution of the drop shape results from the motion of the interface with the fluid velocity \mathbf{v} . The velocity field is nonlinear in \mathbf{f} , but for a given drop shape the boundary-value problems (2)–(4) is linear. Thus, \mathbf{v} can be decomposed into convective and relaxation parts

$$\mathbf{v} = a\dot{\gamma}\mathbf{v}_{\dot{\gamma}} + \mu_1^{-1}\sigma\mathbf{v}_{\sigma}, \tag{6}$$

where the first term represents the velocity field produced by

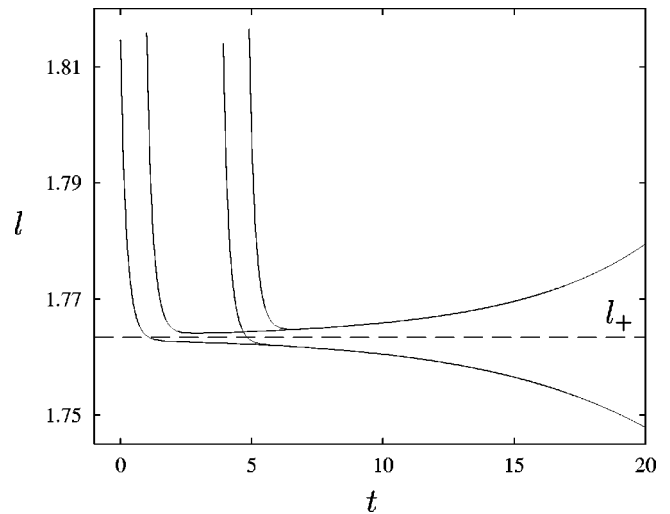


FIG. 2. Short-time evolution of drop length l for initially spheroidal drops ($\eta=1$) in axisymmetric strain, $\kappa/\kappa_C=1.004$. Time-dependent solutions with different initial conditions (solid lines); unstable stationary solution (dashed line).

an incident flow (1) in the absence of capillary forces, and the second term is the capillary-driven fluid velocity in the absence of an incident flow.

Decomposition (6) implies the structure of the evolution equation for the array of shape parameters. In dimensionless variables with time normalized by $\dot{\gamma}^{-1}$ and distances normalized by a , the evolution equation has the form

$$\frac{d\mathbf{f}}{dt} = \mathbf{G}(\mathbf{f}) - \kappa\mathbf{H}(\mathbf{f}), \tag{7}$$

where the function $\mathbf{G}(\mathbf{f})$ results from the convective velocity contribution $\mathbf{v}_{\dot{\gamma}}$, and the function $\mathbf{H}(\mathbf{f})$ is associated with the capillary-driven velocity \mathbf{v}_{σ} .

Explicit expressions for the nonlinear functions \mathbf{G} and \mathbf{H} are known only in the regime of small drop deformations (see Refs. 15 and 16). Outside this regime, \mathbf{G} and \mathbf{H} can be evaluated numerically. In the present work, essential features of drop behavior near critical stationary states are derived from the drop-shape evolution equation in its most general form (7), supplemented by some general assumptions.

III. NEAR-CRITICAL DROP BEHAVIOR

A. Critical capillary parameter

According to experimental and numerical results,¹ for a given viscosity ratio and flow type, there is a range of capillary numbers for which stable stationary drop shapes exist. Typically, stable stationary solutions form a continuous branch $\mathbf{f}_{st} = \mathbf{f}_{st}(\kappa)$ that exists for

$$\kappa > \kappa_C, \tag{8}$$

where κ_C is the critical value of the capillary parameter. Herein, we consider this case.

B. Drop evolution in the near-critical regime

Some general features of drop behavior in the near-critical regime are illustrated in Figs. 1–3, where evolution

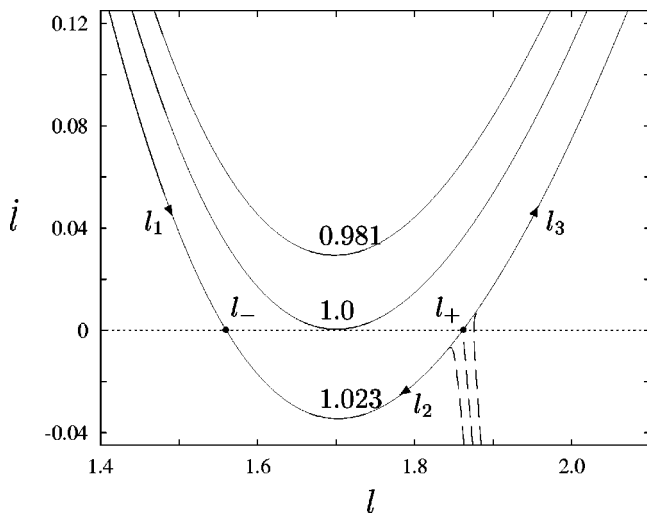


FIG. 3. Rate of change of drop length l versus drop length l for viscous drops ($\eta=1$) in axisymmetric strain. Long-time evolution (solid lines); short-time evolution for different elongated initial drop shapes (dashed lines). Values of κ/κ_C as labeled.

of the drop length, normalized by the drop diameter $2a$, is shown for a drop with $\eta=1$ in axisymmetric straining flow

$$\mathbf{v}_0 = \dot{\gamma}(z\hat{\mathbf{e}}_z - \frac{1}{2}\rho\hat{\mathbf{e}}_\rho). \tag{9}$$

Here (ρ, z) are cylindrical coordinates, and $\hat{\mathbf{e}}_\rho, \hat{\mathbf{e}}_z$ are the corresponding unit vectors. The numerical results presented in Figs. 1–3 were obtained using a boundary-integral algorithm.¹⁷

In Fig. 1(a), drop-length history is shown for a subcritical value of the capillary parameter, $\kappa < \kappa_C$. No stationary states exist in this case, and the length increases continuously (until the drop breaks). In contrast, two stationary drop shapes exist for supercritical values of capillary parameter $\kappa > \kappa_C$, as shown in Fig. 1(b). The results indicate that the stationary shape with the smaller length, $l=l_-$, is stable, and the shape with the larger length, $l=l_+$, is unstable.

The results presented in Fig. 1(b) and the detail of the initial evolution shown in Fig. 2 indicate that the drop evolves on two distinct time scales in the near-critical regime. At short times, evolution occurs on the capillary-relaxation time scale

$$\tau_\kappa = (\kappa\dot{\gamma})^{-1}. \tag{10}$$

Afterwards, the drop evolves on a much longer time scale.

In the long-time regime, drop evolution is insensitive to the details of the initial conditions, as illustrated in Fig. 2. For $\kappa < \kappa_C$ the long-time portion of the trajectory corresponds to a unique sequence of states. For $\kappa > \kappa_C$, after the long-time regime has been achieved, the drop evolves along one of the three trajectories $l=l_i(t)$, where

$$l_1(t) < l_-, \quad l_- < l_2(t) < l_+, \quad l_3(t) > l_+, \tag{11}$$

as seen in Fig. 1.

This behavior is further illustrated in Fig. 3, where the relation between drop length l and its time derivative \dot{l} is shown for a subcritical, critical, and supercritical value of the

capillary parameter. For $\kappa \geq \kappa_C$, the three portions of the continuous curve $\dot{l}(l)$ that correspond to different long-time trajectories $l=l_i(t)$ were obtained using different initial conditions (a sphere for $i=1$, and elongated spheroids with different lengths for $i=2$ and $i=3$).

The results presented in Figs. 1–3 suggest that a saddle-node bifurcation¹⁸ occurs at $\kappa=\kappa_C$. In the following sections, we develop an appropriate phenomenological description.

IV. SLOW MODE DESCRIPTION

A. Expansion of the evolution equation

To characterize drop behavior in the near-critical regime, Eq. (7) is expanded in a Taylor series around the critical stationary shape

$$\mathbf{f}_C = \mathbf{f}_{st}(\kappa_C). \tag{12}$$

A regular expansion in

$$\delta\mathbf{f} = \mathbf{f} - \mathbf{f}_C \tag{13}$$

yields

$$\begin{aligned} \frac{d}{dt}\delta\mathbf{f} = & \mathbf{G}(\mathbf{f}_C) - \kappa\mathbf{H}(\mathbf{f}_C) + [\mathbf{G}^{(1)}(\mathbf{f}_C) - \kappa\mathbf{H}^{(1)}(\mathbf{f}_C)] \cdot \delta\mathbf{f} \\ & + \frac{1}{2}[\mathbf{G}^{(2)}(\mathbf{f}_C) - \kappa\mathbf{H}^{(2)}(\mathbf{f}_C)] : \delta\mathbf{f}\delta\mathbf{f} + \dots, \end{aligned} \tag{14}$$

where $\mathbf{A}^{(i)}$ denotes the i th derivative of \mathbf{A} with respect to \mathbf{f} .

The critical drop shape \mathbf{f}_C is stationary at $\kappa=\kappa_C$, which yields

$$\mathbf{G}(\mathbf{f}_C) - \kappa_C\mathbf{H}(\mathbf{f}_C) = 0. \tag{15}$$

For $\kappa > \kappa_C$ there exist a branch of stationary shapes $\mathbf{f}_{st}(\kappa)$ that are stable to small perturbations, which indicates that all eigenvalues λ_i of the matrix $\mathbf{G}^{(1)}(\mathbf{f}_{st}) - \kappa\mathbf{H}^{(1)}(\mathbf{f}_{st})$ have negative real parts. Based on our numerical results, we assume that only a single mode becomes unstable at the critical state. Accordingly, at $\kappa=\kappa_C$,

$$\lambda_1 = 0 \tag{16}$$

and

$$\text{Re}(\lambda_i) < 0, \quad i=2,3,\dots, \tag{17}$$

where

$$[\mathbf{G}^{(1)}(\mathbf{f}_C) - \kappa_C\mathbf{H}^{(1)}(\mathbf{f}_C)] \cdot \mathbf{g}_i = \lambda_i\mathbf{g}_i, \tag{18}$$

with eigenvectors \mathbf{g}_i forming a (nonorthogonal) basis in the space of shape parameters.

Equations (14)–(18) imply that for $\kappa \approx \kappa_C$ drop-shape perturbations are naturally decomposed as

$$\delta\mathbf{f} = \delta\mathbf{f}_s + \delta\mathbf{f}_f, \tag{19}$$

into the slow mode

$$\delta\mathbf{f}_s = \delta f_s \mathbf{g}_1, \tag{20}$$

and fast modes

$$\delta \mathbf{f}_t = \sum_{i=2}^{\infty} \delta f_i \mathbf{g}_i. \tag{21}$$

The time scale for the evolution of the slow mode diverges for $\kappa \rightarrow \kappa_C$ according to Eq. (16); in contrast, fast modes always evolve on the nonsingular capillary-relaxation time scale (10). This separation of the time scales results in simplified drop dynamics in the near-critical regime: After an initial equilibration on the capillary time scale, fast modes follow the evolution of the slow mode in a quasistatic way, and can thus be eliminated from the evolution equations.

As shown in Appendix 1, the elimination of the fast modes yields a closed evolution equation for the amplitude of the slow mode. To the leading order we obtain

$$\begin{aligned} \frac{d}{dt} \delta \bar{f}_s = \epsilon (-s c_0 + c_2 \delta \bar{f}_s^2) \\ + \epsilon^2 (s c_1 \delta \bar{f}_s + c_3 \delta \bar{f}_s^3) + O(\epsilon^3), \end{aligned} \tag{22}$$

where

$$\epsilon = |\kappa - \kappa_C|^{1/2}, \tag{23}$$

$$s = \text{sign}(\kappa - \kappa_C), \tag{24}$$

$$\delta f_s = \epsilon \delta \bar{f}_s. \tag{25}$$

The constants c_0, \dots, c_3 are given by Eqs. (A11)–(A14) in terms of components of the evolution operators $\mathbf{G}^{(i)}$ and $\mathbf{H}^{(i)}$. A discussion of the higher-order terms in the slow-mode evolution equation (22) is presented in Appendix 2.

B. Dynamics of the slow mode

1. Stationary solutions

According to our assumptions, a stable stationary drop shape exists for $\kappa > \kappa_C$ (i.e., $s = 1$), which yields a constraint

$$c_0/c_2 > 0, \tag{26}$$

for the coefficients in Eq. (22), where $c_0 > 0$ by an appropriate choice of the sign of the basis vector \mathbf{g}_1 .

For $\kappa > \kappa_C$, Eq. (22) has two stationary solutions $\delta \bar{f}_s = h_{\pm}$ that are nonsingular for $\epsilon \rightarrow 0$

$$h_{\pm} = \pm h_0 + \epsilon h_1 + O(\epsilon^2), \tag{27}$$

where

$$h_0 = \left(\frac{c_0}{c_2} \right)^{1/2}, \tag{28}$$

$$h_1 = -\frac{1}{2} \left(\frac{c_1}{c_2} + \frac{c_3}{c_2} h_0^2 \right). \tag{29}$$

As shown in the following subsection, h_- is stable and h_+ is unstable. For $\kappa \rightarrow \kappa_C$ the two stationary drop shapes merge according to (25), and there are no stationary solutions for $\kappa < \kappa_C$.

2. Time-dependent behavior

Integration of Eq. (22) yields implicit relations for the time-evolution of the slow mode. The result, accurate to $O(\epsilon)$, is

$$\epsilon t' = \tau_0 \ln \frac{|\delta \bar{f}_s - h_+|^{g_+(\epsilon)}}{|\delta \bar{f}_s - h_-|^{g_-(\epsilon)}} \tag{30}$$

for $\kappa > \kappa_C$, and

$$\epsilon t' = 2 \tau_0 \arctan[h_0^{-1}(\delta \bar{f}_s + \epsilon h_1)] - \epsilon q \tau_0 \ln(\delta \bar{f}_s^2 + h_0^2) \tag{31}$$

for $\kappa < \kappa_C$, where

$$t' = t - t_0 \tag{32}$$

is the time shifted by the integration constant t_0 ,

$$\tau_0 = \frac{1}{2}(c_0 c_2)^{-1/2}, \tag{33}$$

and

$$g_{\pm}(\epsilon) = 1 \mp q \epsilon \tag{34}$$

with

$$q = c_0^{1/2} c_2^{-3/2} c_3. \tag{35}$$

For small perturbations from the stationary states, Eq. (30) reduces to

$$\delta \bar{f}_s - h_{\pm} \sim \exp(\pm t'/\tau_{\pm}), \tag{36}$$

where the time scale is

$$\tau_{\pm} = \epsilon^{-1} g_{\pm}(\epsilon) \tau_0. \tag{37}$$

Equation (36) indicates that h_- is stable and h_+ is unstable. Drop evolution is slow in the near-critical regime, because the time scales (37) diverge for $\epsilon \rightarrow 0$.

Relations (30) and (31) can be inverted; here we present only the leading-order results. For supercritical values of the capillary parameter, Eq. (30) yields

$$\delta \bar{f}_s = -h_0 \coth(\epsilon t'/\tau_0), \quad \delta \bar{f}_s > h_0; \tag{38}$$

$$\delta \bar{f}_s = -h_0 \tanh(\epsilon t'/\tau_0), \quad -h_0 < \delta \bar{f}_s < h_0. \tag{39}$$

The solution (38) has two branches: the branch $t' > 0$ ($\delta \bar{f}_s < -h_0$) corresponds to trajectory l_1 in Fig. 1, whereas the branch $t' < 0$ ($\delta \bar{f}_s > h_0$) corresponds to trajectory l_3 . The solution (39) has one branch, which corresponds to the trajectory l_2 . For subcritical values of the capillary parameter, Eq. (31) yields

$$\delta \bar{f}_s = h_0 \tan(\epsilon t'/2\tau_0), \tag{40}$$

which has the asymptotic behavior $\delta \bar{f}_s \rightarrow \pm \infty$ for $\epsilon t'/\tau_0 \rightarrow \pm \pi$.

C. Parameter choice

To characterize near-critical drop behavior in computer simulations or in an experiment, an appropriate measurement of the slow-mode amplitude is needed. However, the explicit form of the slow mode is usually unknown or difficult to obtain.

The slow mode decomposition (14)–(21) can be performed analytically for nearly spherical critical drop shapes (e.g., high viscosity drops in near-straining flows), and explicit expressions for the coefficients c_0, \dots, c_3 can be obtained in this case. For higher drop deformations, the linear-perturbation problem (16)–(18) can be solved numerically, but evaluation of higher-order terms would be difficult. Direct experimental measurement of the form of the slow mode is also difficult.

An explicit determination of the slow mode is, however, unnecessary: The critical drop behavior can be observed using any shape parameter

$$l = l(\mathbf{f}) \tag{41}$$

that has a sufficiently strong dependence on $\delta\mathbf{f}_s$.

To characterize the critical behavior of a parameter l , we expand it around the critical shape \mathbf{f}_C . The fast modes $\delta\mathbf{f}_f$ are then eliminated using quasistatic relation (A10). The resulting expansion of l is

$$l = l_C + \epsilon \delta\bar{l}, \tag{42}$$

where

$$l_C = l(\mathbf{f}_C) \tag{43}$$

and

$$\delta\bar{l} = a_1 \delta\bar{f}_s + \epsilon(s a_0 + a_2 \delta\bar{f}_s^2) + O(\epsilon^2), \tag{44}$$

with $a_1 > 0$ assumed. Using relation (44) to eliminate $\delta\bar{f}_s$ from Eq. (22), the long-time evolution equation for the shape parameter $\delta\bar{l}$ is obtained,

$$\frac{d}{dt} \delta\bar{l} = \epsilon(-s b_0 + b_2 \delta\bar{l}^2) + \epsilon^2(s b_1 \delta\bar{l} + b_3 \delta\bar{l}^3) + O(\epsilon^3). \tag{45}$$

This equation has the same form as the slow-mode evolution equation (22). Accordingly, the stationary and time-dependent solutions derived in Sec. IV B apply to $\delta\bar{l}$, after the substitution of the coefficients b_i for c_i .

With an appropriate choice of the shape parameter l , the values of the coefficients b_i can be extracted from experimental or numerical data without a detailed knowledge of the slow mode form. In this paper, critical drop behavior is shown using the drop length (normalized by the diameter $2a$) as the parameter l . Drop length exhibits strong dependence on the critical mode and is convenient to monitor.

V. NUMERICAL RESULTS

Our phenomenological theory has been tested using results of numerical simulations. In Sec. V A, a detailed analysis is given for a drop with $\eta = 1$, in axisymmetric straining flow. Near-critical drop behavior in two-dimensional linear flows is discussed in Sec. V B.

A. Axisymmetric linear flow

Numerical results presented in Sec. III B show that the essential features of our system are consistent with predictions based on the assumption of a saddle-node bifurcation at

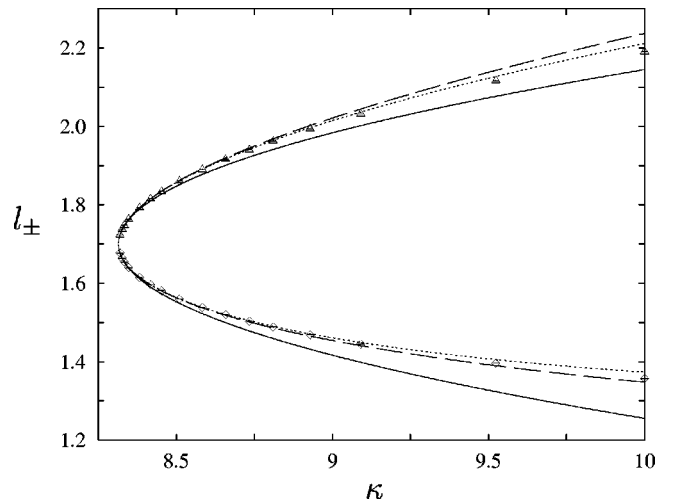


FIG. 4. Stationary drop length versus capillary parameter. Numerical results for stable length l_- (diamonds), unstable length l_+ (triangles). Expansion in powers of ϵ , with expansion coefficients corresponding to solid lines in Fig. 5, truncated at $O(\epsilon)$ (solid line), at $O(\epsilon^2)$ (dashed line), at $O(\epsilon^3)$ (dotted line).

$\kappa = \kappa_C$. Accordingly, after the fast modes are relaxed, the drop evolution is fully characterized by the amplitude of a single slow mode. The critical capillary number corresponds to $\dot{l} = 0$ at the minimum of the phase-space relation $\dot{l} = \dot{l}(l)$. For $\kappa > \kappa_C$, there is one stable and one unstable stationary state.

In the remaining part of the present section, we describe detailed quantitative tests of the theory.

1. Drop behavior near stationary states

We first consider the stable and unstable stationary drop lengths l_- and l_+ . Stationary lengths versus capillary parameter are shown unscaled in Fig. 4, and rescaled in Fig. 5. As discussed in Appendix 2, the rescaled stationary length difference

$$d = \frac{1}{2} \epsilon^{-1} (l_+ - l_-), \tag{46}$$

and the average length

$$L = \frac{1}{2} (l_+ + l_-), \tag{47}$$

are regular functions of κ . Numerical results shown in Fig. 5 are consistent with this behavior. The linear asymptotic form of d , as plotted in Fig. 5(a), corresponds to

$$\kappa_C = 8.315. \tag{48}$$

The lines in Figs. 5(a) and 5(b) represent the asymptotic behavior

$$d = l_1 + l_3(\kappa - \kappa_C), \quad L = l_0 + l_2(\kappa - \kappa_C), \tag{49}$$

where the values

$$l_0 = 1.700 \tag{50}$$

for the critical length, and $l_1 = 0.3426$, $l_2 = 0.0548$, $l_3 = -0.0117$ are obtained by matching to the numerical data.

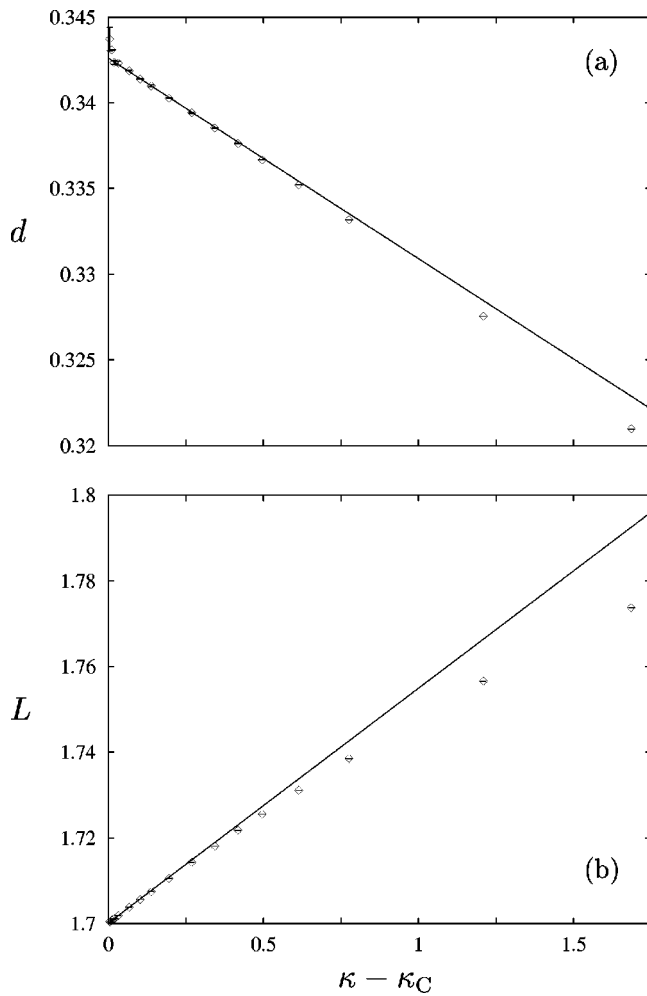


FIG. 5. Rescaled drop length difference (a), and average drop-length (b), versus $\kappa - \kappa_C$. Numerical results (diamonds); asymptotic behavior (49) (solid lines).

The results (48) and (50) are consistent with the values reported by Navot.¹³ The approximations accurate up to $O(\epsilon^3)$ for l_- and l_+ , with the coefficients given above, are shown in Fig. 4.

Next we consider the inverse time scales

$$\alpha_{\pm} = \pm \tau_{\pm}^{-1}, \tag{51}$$

which characterize the slow-mode behavior (36) near the stable and unstable stationary states. These time scales, obtained from an analysis of the exponential evolution of the drop length for $l \approx l_{\pm}$, are shown unscaled in Fig. 6, and rescaled in Fig. 7.

The behavior of the time scales in the near-critical regime is analogous to the behavior of the stationary drop lengths. The rescaled quantities

$$\delta = \frac{1}{2} \epsilon^{-1} (\alpha_+ - \alpha_-) \tag{52}$$

and

$$A = \frac{1}{2} (\alpha_+ + \alpha_-) \tag{53}$$

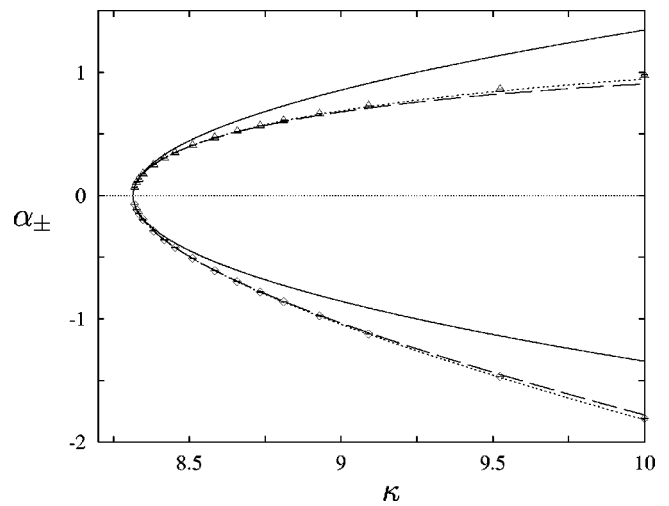


FIG. 6. Inverse time scale (51) for the evolution near the stable and unstable stationary states. The meaning of symbols as in Fig. 4, except that the results are for α_{\pm} , and the expansion coefficients correspond to the lines in Fig. 7.

are regular in κ , as discussed in Appendix 2 and illustrated in Fig. 7. The rescaled time-scale difference (52) shown in Fig. 7(a) corresponds to the critical value (48) of the capillary parameter, consistently with the stationary

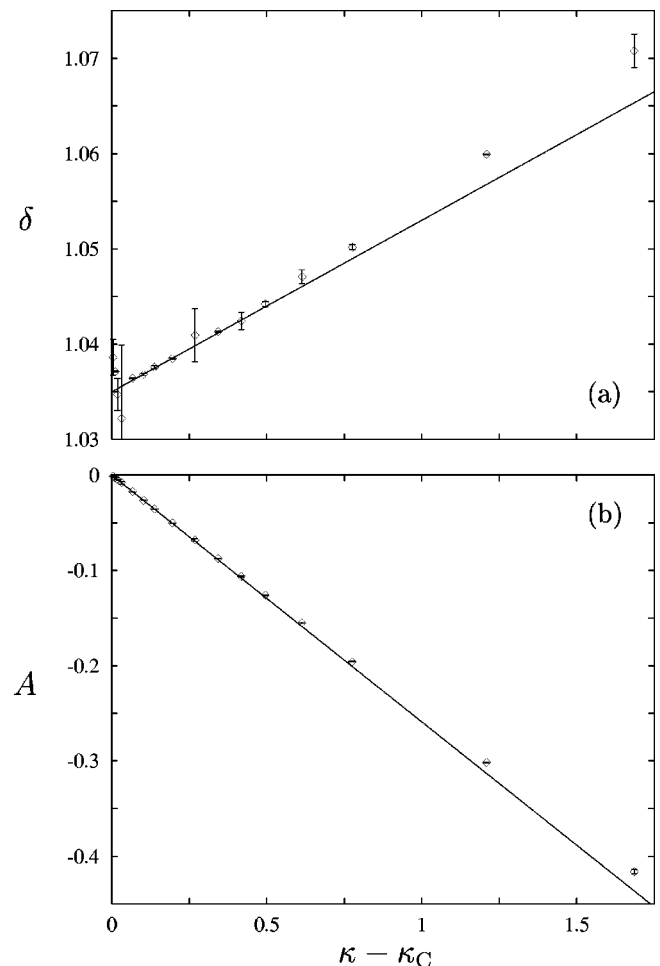


FIG. 7. Rescaled inverse time scale difference (a), and average inverse time scale (b), versus $\kappa - \kappa_C$. Numerical results (diamonds); asymptotic behavior (54) (solid lines).

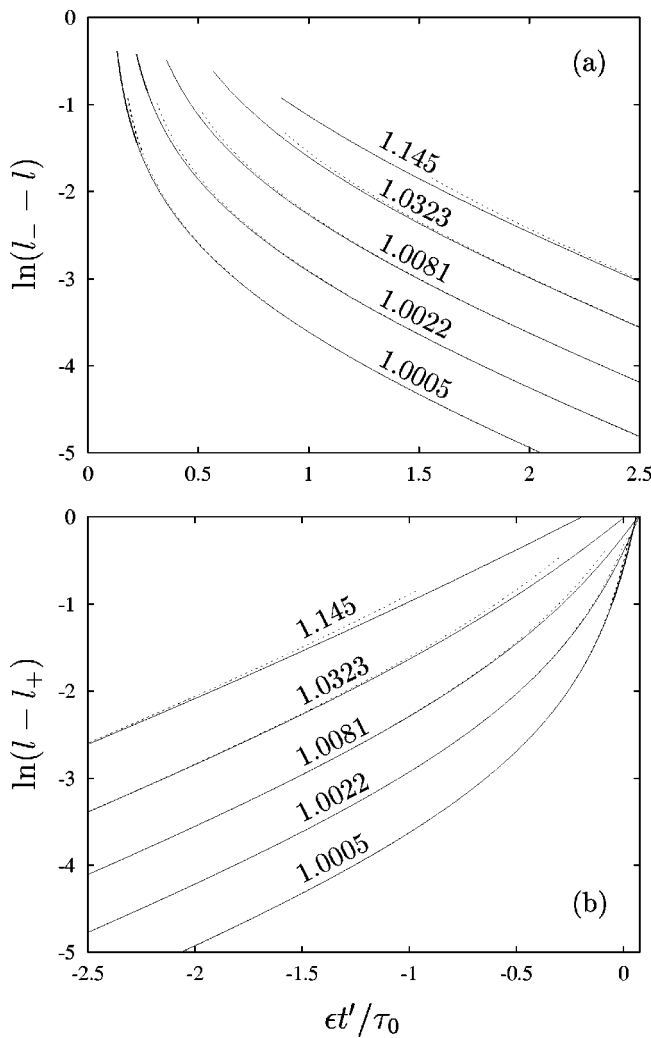


FIG. 8. Drop length versus rescaled time for $l < l_-$ (a), and $l > l_+$ (b). Numerical results (solid lines); expression (30) (dotted lines). Values of κ/κ_C as labeled.

results. The lines in Figs. 7(a) and 7(b) represent the asymptotic behavior

$$\delta = \alpha_1 + \alpha_3(\kappa - \kappa_C), \quad A = \alpha_2(\kappa - \kappa_C), \quad (54)$$

where $\alpha_1 = 1.035$, $\alpha_2 = -0.259$, and $\alpha_3 = 0.018$. (The value reported by Navot¹³ for the coefficient corresponding to α_1 is 20% smaller.)

The error bars in Figs. 4–7 represent numerical errors estimated by comparing the values of l_{\pm} and α_{\pm} obtained from analyses of the dynamics just below and just above the stable and unstable stationary states. In most cases, the error bars are invisible on the scale of the figures, except in Figs. 5(a) and 7(a), where the inaccuracies are magnified by the factor ϵ^{-1} in Eqs. (46) and (52). Occasional large error bars reflect numerical noise generated by interface remeshing.

2. Drop evolution

The theoretical predictions given in Sec. IV B 2 will now be compared to our numerical results for the drop-length evolution.

For $\kappa > \kappa_C$, we focus on the intermediate long-time regime, where the evolution predicted by Eq. (30) (with slow-

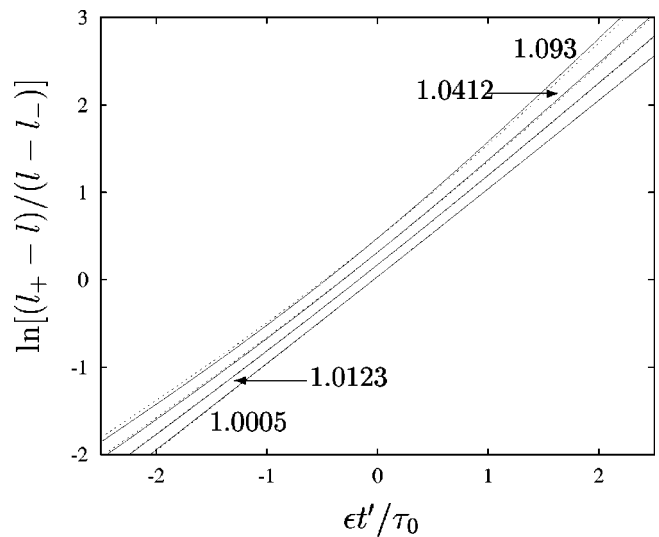


FIG. 9. Same as Fig. 8, except that $l_- < l < l_+$.

mode parameter δf_s represented by drop length l) is nonexponential. Exact values were used for the parameters l_{\pm} and α_{\pm} , as determined from the long-time asymptotic behavior (36). The comparison between approximation (30) and the numerical results is presented in Figs. 8 and 9.

The results for $l < l_-$ are shown in Fig. 8(a). Time is shifted so that Eq. (30) and the numerical values coincide for large t' . The left ends of the curves representing the simulation correspond to the initial spherical drop shape. The theoretical curves for the slow-mode evolution are truncated at $t' = 4\tau_{\kappa}$.

The results for $l > l_+$ are shown in Fig. 8(b). Here, time is shifted so that Eq. (30) and the numerical values coincide for large negative values of t' . For $t' \rightarrow 0$, the theoretical curves are truncated for $l/l_0 > 1.5$, where l_0 is the critical length (50).

The results corresponding to the nonlinear portions of the curves indicate that approximation (30) is valid in the nonexponential regimes, provided that fast modes have relaxed, and the perturbation from the critical state is sufficiently small. (By construction, the numerical results and the asymptotic predictions coincide in the exponential regimes $t \rightarrow \pm \infty$.)

Figure 9 presents drop evolution for $l_- < l < l_+$. In this case, a transition between two exponential asymptotic behaviors occurs; accordingly, the plot of $\ln[(l_+ - l)/(l - l_-)]$ is shown. Time is shifted so that the numerical and theoretical curves match at $t' = 0$. The results indicate that approximation (30) is accurate up to moderate values of $\kappa - \kappa_C$.

For $\kappa < \kappa_C$, there are no stationary drop shapes. In this regime, numerical results for drop length are compared to the leading-order solution (40) and the first-order solution (31), with parameter values obtained from the expansions (49) and (54). The plot of drop length versus the rescaled time is shown in Fig. 10 for several values of the capillary parameter.

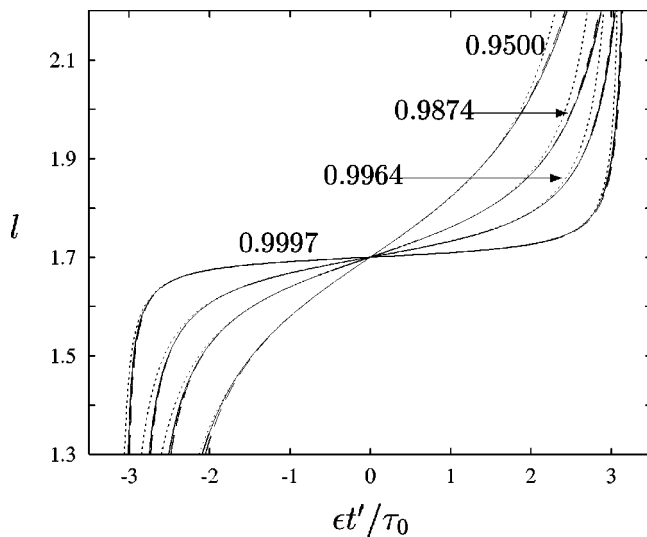


FIG. 10. Drop length versus rescaled time. Numerical results (solid line); leading-order approximation (dotted line); first-order approximation (dashed line). Values of κ/κ_C as labeled.

B. Two-dimensional linear flows

We performed three-dimensional boundary integral simulations¹⁹ of drop evolution in two-dimensional linear flows

$$\mathbf{v}_0 = \frac{1}{2} \dot{\gamma} [(1 + \beta)y \hat{\mathbf{e}}_x + (1 - \beta)x \hat{\mathbf{e}}_y], \tag{55}$$

where β is the vorticity parameter, (x, y, z) are Cartesian coordinates, and $\hat{\mathbf{e}}_x, \hat{\mathbf{e}}_y$ are unit vectors in the x and y directions. Expression (55) with $\beta=1$ corresponds to a shear flow in x direction and $\beta=0$ to a two-dimensional strain. Examples illustrating typical near-critical drop behavior in flows (55) are shown in Figs. 11 and 12 for $\beta=0.9$ and viscosity ratio $\eta=1$.

Figure 11 illustrates evolution of initially spherical drops with $\kappa > \kappa_C$ toward the stable stationary state. The results are

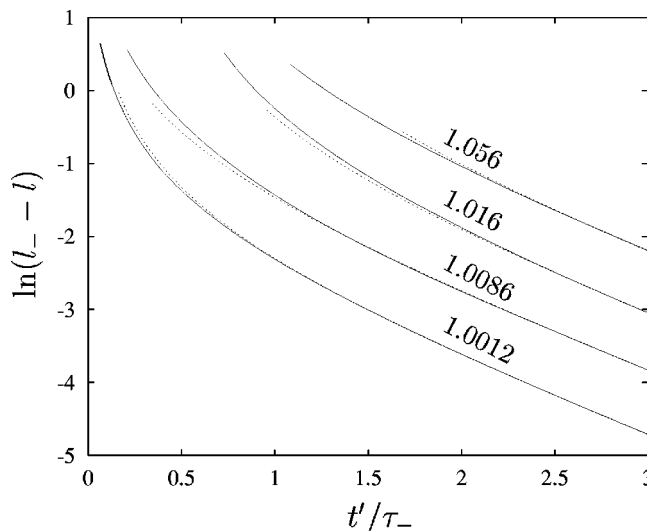


FIG. 11. Evolution of drop length in linear flow (55) with $\beta=0.9$ and viscosity ratio $\eta=1$ in the regime $l < l_-$. Numerical results (solid lines); expression (30) (dotted lines). Values of κ/κ_C as labeled.

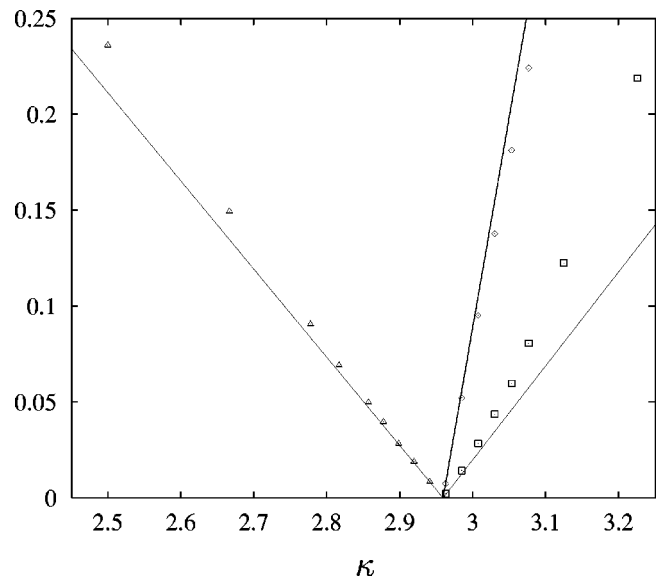


FIG. 12. Stable stationary drop length difference Δl^2 (diamonds), inverse square relaxation time α_-^2 (squares), and minimum elongation rate \dot{l}_{\min} (triangles) versus capillary parameter κ . Results from boundary-integral simulations in two-dimensional flow (55) with $\beta=0.9$ and viscosity ratio $\eta=1$. Solid lines depict the linear asymptotic behaviors (57) and (59).

analogous to those shown in Fig. 8(a) for the axisymmetric straining flow. Within the resolution of our three-dimensional simulations, we were able to determine only the leading-order coefficient τ_0 in the expansion of the characteristic time τ_- . Thus, the leading-order approximation $g_{\pm}(\epsilon) = 1$ was used in the plot of theoretical expression (30). For the unstable stationary length we used $l_+ = 2l_0 - l_-$, which is the leading-order term in the expansion (49) of the length difference d . The results in the nonlinear range of the curves, corresponding to drop behavior for moderate times, are sensitive to the values of parameters l_- and l_0 . These parameters were obtained from the analysis of the long-time behavior of the drop length. The scatter of the results in the nonlinear range stems from numerical inaccuracies.

For $\kappa > \kappa_C$, Fig. 12 shows the κ dependence of the inverse square relaxation time α_-^2 and the stationary-length parameter

$$\Delta l^2 = (l_- - l_0)^2 \tag{56}$$

(where the same value of l_0 was used as in Fig. 11). At leading order these quantities are linear in $\delta\kappa = \kappa - \kappa_C$,

$$\begin{aligned} \alpha_-^2 &= \alpha_1^2 \delta\kappa + O(\delta\kappa^{3/2}), \\ \Delta l^2 &= l_1^2 \delta\kappa + O(\delta\kappa^{3/2}), \end{aligned} \tag{57}$$

according to Eqs. (52)–(54) and (46), (47), (49). For $\kappa < \kappa_C$, Fig. 12 shows the minimal elongation rate on a drop trajectory

$$\dot{l}_{\min} = \min(dl/dt), \tag{58}$$

which behaves as

$$\dot{l}_{\min} = b_0 \delta\kappa + O(\delta\kappa^2), \tag{59}$$

according to Eq. (45). Within numerical accuracy, the straight lines representing the asymptotic behaviors (57) and (59) correspond to the same value of the critical capillary parameter $\kappa_C = 2.96$.

The results shown in Figs. 11 and 12, as well as numerical simulations for other values of the viscosity ratio η and vorticity parameter β (up to $\beta = 0.98$), show that the saddle-node bifurcation mechanism described in the present paper holds for drops in two-dimensional linear flows with $\beta < 1$. However, numerical results for drops in shear flow ($\beta = 1$) suggest that the near-critical behavior may be distinct. These results indicate that away from the near-critical regime drops in shear exhibit damped oscillations associated with two complex conjugate modes,²⁰ although we were unable to determine whether the eigenvalues remain complex or become real as κ approaches the critical value.

VI. CONCLUSIONS

Our study provides a phenomenological framework for describing the dynamics of drops in creeping flows under near-critical conditions. In the near-critical regime, drop behavior is dominated by the evolution of a single slow mode, and at the critical point the system undergoes a saddle-node bifurcation. Thus, the transient dynamics and stationary states are characterized by the classical critical exponent 1/2, in analogy to the Landau theory of phase transitions. Our theory is useful for accurately extracting critical parameter values from numerical simulations and experimental data using, e.g., asymptotic relations (57) and (59).

The predicted bifurcation mechanism has been verified by numerical simulations for drops in axisymmetric straining flow and in two-dimensional flows with rotation parameter $\beta \leq 0.98$. We expect that our theory applies to a broad class of flow types, with possible exceptions such as simple shear flow, where a different mechanism may occur according to our numerical simulations.

In linear flows with nonzero vorticity, drop rotation provides a stabilizing mechanism even in the absence of capillary forces.^{16,21} As a result, there exists a critical viscosity ratio η_C , such that for $\eta < \eta_C$ (high-viscosity drops) stationary states occur at arbitrary strain rates. An extension of our formalism to describe the near-critical behavior of drops for $\eta \approx \eta_C$, as well as the dependence of η_C on the flow type, will be presented elsewhere.

In a recent presentation,²² multiple stable stationary states were shown to occur for high-viscosity drops in two-dimensional flows with weak vorticity. Under these conditions, there exists a branch of stationary solutions that is limited at both ends, $\kappa'_C > \kappa > \kappa_C$, in contrast to Eq. (8). With minor modifications, the theory developed herein applies to both near-critical regions $\kappa \approx \kappa_C, \kappa'_C$.

Our approach may be useful for analyzing the dynamics of polymer molecules undergoing coil–stretch transitions in external flows.^{23,24} These transitions result from the interplay between entropically driven relaxation and convection by an imposed flow.²⁵ The essential mechanism is thus similar to the one studied herein.

ACKNOWLEDGMENTS

J.B. was supported by NSF Grant No. CTS-9624615 and NASA Grant No. NAG3-2704; V.C. was supported by NASA Grant No. NAG3-1935.

APPENDIX: EVOLUTION EQUATION FOR THE SLOW MODE

1. Derivation of Eq. (22)

Two coupled evolution equations for the slow and the fast modes are derived by applying to both sides of Eq. (14) projection operators \hat{P}_s and \hat{P}_f onto subspaces (20) and (21)

$$\begin{aligned} \frac{d}{dt} \delta \mathbf{f}_s = & -\delta \kappa \mathbf{H}_s - \delta \kappa \mathbf{H}_s^{(1)} \cdot \delta \mathbf{f} \\ & + \frac{1}{2} (\mathbf{B}_s^{(2)} - \delta \kappa \mathbf{H}_s^{(2)}) : \delta \mathbf{f} \delta \mathbf{f} + \dots, \end{aligned} \quad (A1)$$

$$\begin{aligned} \frac{d}{dt} \delta \mathbf{f}_f = & -\delta \kappa \mathbf{H}_f + \mathbf{B}_f^{(1)} \cdot \delta \mathbf{f}_f - \delta \kappa \mathbf{H}_f^{(1)} \cdot \delta \mathbf{f} \\ & + \frac{1}{2} (\mathbf{B}_f^{(2)} - \delta \kappa \mathbf{H}_f^{(2)}) : \delta \mathbf{f} \delta \mathbf{f} + \dots, \end{aligned} \quad (A2)$$

where $\delta \kappa = \kappa - \kappa_C$,

$$\mathbf{B}^{(i)} = \mathbf{G}^{(i)} - \kappa_C \mathbf{H}^{(i)}, \quad (A3)$$

and

$$\mathbf{A}_a = \hat{P}_a \mathbf{A}, \quad a = s, f \quad (A4)$$

(with $\mathbf{A} = \mathbf{f}, \mathbf{H}, \mathbf{B}, \dots$). The operators $\mathbf{G}, \mathbf{H}, \mathbf{B}$ are evaluated at $\mathbf{f} = \mathbf{f}_C$. Equations (A1) and (A2) were simplified using relation (15), and the identities

$$\mathbf{B}_s^{(1)} \mathbf{f} = 0, \quad \mathbf{B}_f^{(1)} \mathbf{f}_s = 0. \quad (A5)$$

These identities follow from (16) and the observation that the subspaces \mathbf{f}_s and \mathbf{f}_f correspond to different eigenvalues of the operator $\mathbf{B}^{(1)}$.

Equation (A2) indicates that, at the leading order in $\delta \kappa$, the evolution of the fast mode near the stationary state is governed by the constant term $-\delta \kappa \mathbf{H}_f$ and the linear term $\mathbf{B}_f^{(1)} \cdot \delta \mathbf{f}_f$. In contrast, the linear term is missing from Eq. (A1) at the leading order; thus, the evolution of the slow mode is governed by the constant term and the quadratic term in $\delta \mathbf{f}_s$. Accordingly, the following scalings are appropriate for the slow and the fast modes

$$\delta \mathbf{f}_s = \epsilon \delta \bar{\mathbf{f}}_s, \quad (A6)$$

$$\delta \mathbf{f}_f = \epsilon^2 \delta \bar{\mathbf{f}}_f, \quad (A7)$$

where ϵ is given by Eq. (23). In the rescaled variables, the leading-order terms in the evolution equations for the slow and the fast modes are

$$\begin{aligned} \frac{d}{dt} \delta \bar{\mathbf{f}}_s = & \epsilon (-s \mathbf{H}_s + \frac{1}{2} \mathbf{B}_s^{(2)} : \delta \bar{\mathbf{f}}_s \delta \bar{\mathbf{f}}_s) + \epsilon^2 (-s \mathbf{H}_s^{(1)} \cdot \delta \bar{\mathbf{f}}_s \\ & + \mathbf{B}_s^{(2)} : \delta \bar{\mathbf{f}}_f \delta \bar{\mathbf{f}}_s + \frac{1}{6} \mathbf{B}_s^{(3)} : \delta \bar{\mathbf{f}}_s \delta \bar{\mathbf{f}}_s \delta \bar{\mathbf{f}}_s) + O(\epsilon^3), \end{aligned} \quad (A8)$$

$$\begin{aligned} \frac{d}{dt} \delta \bar{\mathbf{f}}_f = & -s \mathbf{H}_f + \mathbf{B}_f^{(1)} \cdot \delta \bar{\mathbf{f}}_f \\ & + \frac{1}{2} \mathbf{B}_f^{(2)} : \delta \bar{\mathbf{f}}_s \delta \bar{\mathbf{f}}_s + O(\epsilon), \end{aligned} \quad (\text{A9})$$

where s is defined by (24).

Equation (A8) indicates that the evolution of the slow mode occurs on a time scale that diverges at $\kappa \rightarrow \kappa_C$ with critical exponent 1/2. At leading order, the equation for the slow mode is independent of the fast modes, but at the order $O(\epsilon^2)$, the slow and fast modes are coupled. However, on the time scale $t = O(1)$, fast modes relax towards the quasi-stationary solution of Eq. (A9)

$$\delta \bar{\mathbf{f}}_f = \mathbf{B}_f^{(1)-1} \cdot (s \mathbf{H}_f - \frac{1}{2} \mathbf{B}_f^{(2)} : \delta \bar{\mathbf{f}}_s \delta \bar{\mathbf{f}}_s) + O(\epsilon), \quad (\text{A10})$$

and then follow the evolution of the slow mode adiabatically. Inserting the above expression into Eq. (A8) yields the closed long-time evolution equation (22) for the slow mode, where

$$c_0 \mathbf{g}_1 = \mathbf{H}_s, \quad (\text{A11})$$

$$c_1 \mathbf{g}_1 = [-\mathbf{H}_s^{(1)} + \mathbf{B}_s^{(2)} \cdot (\mathbf{B}_f^{(1)-1} \cdot \mathbf{H}_f)] \cdot \mathbf{g}_1, \quad (\text{A12})$$

$$c_2 \mathbf{g}_1 = \frac{1}{2} \mathbf{B}_s^{(2)} : \mathbf{g}_1 \mathbf{g}_1, \quad (\text{A13})$$

$$c_3 \mathbf{g}_1 = [\frac{1}{6} \mathbf{B}_s^{(3)} - \frac{1}{2} \mathbf{B}_s^{(2)} \cdot (\mathbf{B}_f^{(1)-1} \cdot \mathbf{B}_f^{(2)})] : \mathbf{g}_1 \mathbf{g}_1 \mathbf{g}_1. \quad (\text{A14})$$

2. Higher-order terms

Elimination of the fast modes can be continued to arbitrary order. This procedure yields a slow-mode evolution equation of the form

$$\epsilon \frac{d}{dt} \delta \bar{f}_s = \epsilon^2 (-s c_0 + c_2 \delta \bar{f}_s^2) + \epsilon^3 \psi(\delta \bar{f}_s; \epsilon), \quad (\text{A15})$$

with ψ given as a series in $\delta \bar{f}_s$ and ϵ .

The unscaled evolution equations (A1) and (A2) are regular in κ and δf_s . The odd powers of ϵ in Eq. (A15) result from the rescaling of the slow-mode amplitude (A6). As a consequence, the function ψ satisfies the symmetry relation

$$\psi(-\delta \bar{f}_s; -\epsilon) = -\psi(\delta \bar{f}_s; \epsilon), \quad (\text{A16})$$

since the unscaled array $\delta \bar{\mathbf{f}}_s$ is invariant under a simultaneous change of sign of ϵ and $\delta \bar{\mathbf{f}}_s$ in Eq. (A6).

The nonsingular stationary solutions $\delta \bar{f}_s = h_{\pm}$ of the slow-mode evolution equation are related by

$$h_+(\epsilon) = -h_-(\epsilon), \quad (\text{A17})$$

which can be shown by inserting the result into (A15), and using symmetry relation (A16). Equation (A17) implies that $\frac{1}{2}(h_+ - h_-)$ and $\frac{1}{2}\epsilon(h_+ + h_-)$ are symmetric functions of ϵ , and thus have regular expansions in $\epsilon^2 = \kappa - \kappa_C$. The corresponding even-power expansions of Eqs. (46) and (47) follow.

Perturbing Eq. (A15) around the stationary solutions $\delta \bar{f}_s = h_{\pm}$ yields the inverse time scales (51)

$$\alpha_{\pm} = 2\epsilon c_2 h_{\pm} + \epsilon^2 \psi'(h_{\pm}, \epsilon), \quad (\text{A18})$$

where the prime denotes the derivative with respect to $\delta \bar{f}_s$. Symmetry relations (A16) and (A17) thus imply that

$$\alpha_+(\epsilon) = \alpha_-(\epsilon), \quad (\text{A19})$$

from which it follows that (52) and (53) have regular expansions in ϵ^2 .

¹H. A. Stone, "Dynamics of drop deformation and breakup in viscous fluids," *Annu. Rev. Fluid Mech.* **26**, 65 (1994).

²J. P. Grace, "Dispersion phenomena in high viscosity immiscible fluid systems and application of static mixers as dispersion devices in such systems," *Chem. Eng. Commun.* **14**, 225 (1982).

³B. J. Bentley and L. G. Leal, "An experimental investigation of drop deformation and breakup in steady, two-dimensional linear flows," *J. Fluid Mech.* **167**, 241 (1986).

⁴R. A. Bruijn, Ph.D. thesis, Tech. Univ. Eindhoven (1989).

⁵M. R. Kennedy, C. Pozrikidis, and R. Skalak, "Motion and deformation of liquid drops and the rheology of dilute emulsions in simple shear flow," *Comput. Fluids* **23**, 251 (1994).

⁶J. Li, Y. Y. Renardy, and M. Renardy, "Numerical simulation of breakup of a viscous drop in simple shear flow through a volume-of-fluid method," *Phys. Fluids* **12**, 269 (2000).

⁷H. A. Stone and L. G. Leal, "Relaxation and breakup of an initially extended drop in an otherwise quiescent fluid," *J. Fluid Mech.* **198**, 399 (1989).

⁸M. Tjahjadi and J. M. Ottino, "Stretching and breakup of droplets in chaotic flows," *J. Fluid Mech.* **232**, 191 (1991).

⁹F. J. Muzzio, M. Tjahjadi, and J. M. Ottino, "Self-similar drop-size distributions produced by breakup in chaotic flows," *Phys. Rev. Lett.* **67**, 54 (1991).

¹⁰J. M. H. Janssen and H. E. H. Meijer, "Droplet breakup mechanisms: Stepwise equilibrium versus transient dispersion," *J. Rheol.* **37**, 597 (1993).

¹¹D. I. Bigio, C. R. Marks, and R. V. Calabrese, "Predicting drop breakup in complex flows from model flow experiments," *Int. Polym. Process.* **13**, 192 (1998).

¹²C. R. Marks, Ph.D. thesis, University of Maryland at College Park (1998).

¹³Y. Navot, "Critical behavior of drop breakup in axisymmetric viscous flow," *Phys. Fluids* **11**, 990 (1999).

¹⁴J. Bławdziewicz, V. Cristini, and M. Loewenberg, "Critical conditions for drop breakup in linear flows," *Bull. Am. Phys. Soc.* **43**, 2066 (1998).

¹⁵D. Barthès-Biesel and A. Acrivos, "Deformation and burst of a liquid droplet freely suspended in a linear shear field," *J. Fluid Mech.* **61**, 1 (1973).

¹⁶J. M. Rallison, "Note on the time-dependent deformation of a viscous drop which is almost spherical," *J. Fluid Mech.* **98**, 625 (1980).

¹⁷C. Pozrikidis, *Boundary Integral and Singularity Methods for Linearized Viscous Flow* (Cambridge University Press, Cambridge, 1992).

¹⁸P. G. Drazin, *Nonlinear Systems* (Cambridge University Press, Cambridge, 1992).

¹⁹V. Cristini, J. Bławdziewicz, and M. Loewenberg, "An adaptive mesh algorithm for evolving surfaces: Simulations of drop breakup and coalescence," *J. Comput. Phys.* **168**, 445 (2001).

²⁰E. H. Hinch and A. Acrivos, "Long slender drops in a simple shear flow," *J. Fluid Mech.* **98**, 305 (1980).

²¹G. I. Taylor, "The formation of emulsions in definable fields of flow," *Proc. R. Soc. London, Ser. A* **146**, 501 (1934).

²²J. Bławdziewicz, V. Cristini, and M. Loewenberg, "Near-critical behavior and critical conditions for drop breakup in linear flows with rotation," *Bull. Am. Phys. Soc.* **44**, 98 (1999).

²³D. E. Smith, H. P. Babcock, and S. Chu, "Single-polymer dynamics in steady shear flows," *Science* **283**, 1724 (1999).

²⁴P. LeDuc, C. Haber, G. Bao, and D. Wirtz, "Dynamics of individual flexible polymers in a shear flow," *Nature (London)* **399**, 564 (1999).

²⁵P. G. de Gennes, "Coil-stretch transition of dilute flexible polymers under ultrahigh velocity gradients," *J. Chem. Phys.* **60**, 5030 (1974).